ACS APPLIED MATERIALS & INTERFACES

Research Article

www.acsami.org

Impact of Nanoparticle Aggregation on Protein Recovery through a Pentadentate Chelate Ligand on Magnetic Carriers

P. Fraga García, M. Freiherr von Roman, S. Reinlein, M. Wolf, and S. Berensmeier*

Bioseparation Engineering Group, Mechanical Engineering Faculty, Technische Universität München, Boltzmannstrasse 15, D-85748 Garching, Germany

Supporting Information

ABSTRACT: The growing need for more efficient separation techniques still dominates downstream processing of biomolecules, thus encouraging the continuous development of advanced nanomaterials. In this paper we present an improved process for recovering recombinant histidine tagged green fluorescent protein from an *E. coli* cell lysate. Superparamagnetic core−shell nanocarriers are functionalized with a pentadentate chelate affinity ligand and then loaded with metal ions (Cu^{2+}, Ni^{2+}, or Zn^{2+}). The separation process yields high binding capacity (250 mg/g), good selectivity, purity >98%, good recyclability with 90% capacity after 9 cycles, and long-term stability. We determined the main physical properties of the magnetite-based nanoparticles such as saturation magnetization (59 A m^2/kg), primary particle diameter (22 ± 4 nm), and specific surface area (89 m^2/g). Our results show that this material is a promising tool for bioseparation applications. One special focus of the work includes analyzing the changes in the hydrodynamic size distribution using dynamic light scattering and transmission electron microscopy. We relate these effects to different interaction levels in the system and discuss how the stronger aggregation of the magnetite core is the main limiting factor for the separation yield, leading to a considerable decrease in the number of metal ions available for biomolecular capture. Otherwise weaker interactions lead instead to agglomeration effects that have no impact on the binding capacity of the system. The simple relation between the size of the aggregated units and the size of the primary particles corresponds approximately to the relation between the number of existing binding sites and the actual protein binding in the separation process. Compared with that, the effect of steric hindrance among proteins is of less significance.

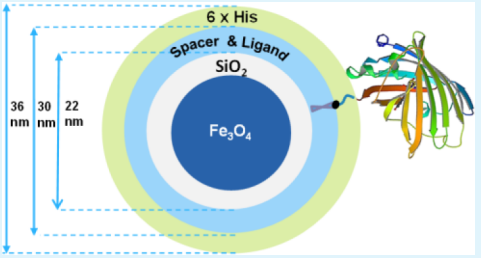

KEYWORDS: *protein recovery, biomolecule purification, magnetic separation, pentadentate chelate ligand, aggregation, agglomeration, nanoparticles*

1. INTRODUCTION

The increasing demand for efficient and selective techniques for separation and purification of biomolecules also requires the continuous development of new materials with optimized properties for an easy, fast, and effective capture step. In this context, taking advantage of nanostructures provides plenty of possibilities for modern biotechnological investigation, at the same time bringing with it new challenges to be solved.

Selective protein isolation from a fermentation broth is currently carried out using affinity tags, which are genetically attached to the target protein to enable a higher specificity for concrete ligands. Porath[1] was the pioneer of the immobilized metal ion affinity chromatography (IMAC) or also metal chelate affinity chromatography; many reviews report on the purification of proteins by IMAC.[2,3] Lönnerdal and Keen[4] listed the main advantages of this method as (1) high capacity, (2) quantitative recovery, (3) no damage to the protein, and (4) easy regeneration. The principle is based on the fact that many transition metal ions form coordination bonds with oxygen, nitrogen, and sulfur atoms in amino acid side chains. The metal ion must be immobilized on an insoluble carrier, which can be easily achieved by building a complex with a chelating ligand that is covalently bound to the carrier. Two ligands are usually applied in all immobilized metal ion affinity (IMA) techniques: the tridentate ligand iminodiacetic acid (IDA)[5,6] and the tetradentate nitrilotriacetic acid (NTA)[7,8]. Among all amino acids histidine (His) shows the strongest interaction with immobilized metal ions, through coordination of the transition metal with the free nitrogen electrons of the histidine ring.[9] Thus, genetic modification through the addition of histidine residues to the protein enhances its affinity for metal ions. Typically, six or eight consecutive residues are enough for the recombinant protein to have a considerably higher affinity for metal ions than other host cell proteins. In the meantime, IMA techniques have become a very important tool in molecular biology, in particular for the separation of histidine-tagged proteins.[10]

Pentadentate ligands such as tris(carboxymethyl)-ethylenediamine, TED,[11] and ethylenediaminetetraacetic acid, EDTA,[12,13] represent an additional interesting group of ligands. For EDTA in particular a higher selectivity for His-tagged proteins in comparison to tri- and tetradentate ligands is

Received: May 19, 2014
Accepted: August 4, 2014
Published: August 4, 2014

suspected, as recently reported by GE Healthcare.[14] Andersson and collaborators suppose the metal ion to generally interact weaker with all proteins because of the lower number of free coordination sites; therefore, a higher selectivity for tagged proteins could be realized in a kind of competitive binding with a positive effect for stronger binders, e.g. histidine units. Two other advantages of pentadentate ligands are related to the lower metal leaching during the separation process; due to the stronger interaction between ligand and metal ion (1) there is a decrease in contamination of the main protein and (2) an improvement in the recyclability of the adsorbers. In the last five to ten years, some patents have been accepted related to novel metal ligands for His-tagged biomolecules, mainly from GE Healthcare,[15,16] but, as far as we know, no scientific articles related to these patents have been published yet.

The impressive development of nanoscience in the last decades has been accompanied by a continuously growing interest in magnetic nanoparticles (MNPs), a tendency also observed in downstream processing.[17] The facile separation under the magnetic field together with their biocompatibility offers a broad range of possibilities for MNPs as carriers for biomolecules. They are often produced as hybrid nanostructures in the form of a core−shell system to prevent further oxidation, to enable easier functionalization, and to enhance their stability in the aqueous environment. Much work focuses on the synthesis of magnetic colloidal systems, including pure iron oxide particles as well as hybrid materials.[18−22] For optimal separation ability, the MNPs should be superparamagnetic and have high effective specific areas. Selective binding properties are achieved using functional groups attached to their surface. One of the main problems concerns suspension stability: because of their high surface-to-volume ratios and because of their magnetism, MNPs strongly tend to agglomerate, therefore often reducing the available area for a successful interaction with the target material. In this context, the challenge is still to find ways of stabilizing primary nanostructures with a completely accessible surface for the adsorption process and still adequate agglomeration grade to secure the fast and easy separation by magnetic forces.

Nowadays some scientific research is being carried out on biomolecular capture by immobilized metal ions on magnetic carriers.[23] Most published works employ the classical tri-[24−26] and tetradentate[27,28] metal chelate ligands to take advantage of their high binding capacity. With pentadentate ligands selectivity can be enhanced, sometimes at the expense of the stability because of the weaker interactions of the metal ion complex with the target molecules.[14] However, in this paper we prove that the immobilized pentadentate chelate ligand EDTA shows very good selectivity as well as enough stability and also a high capacity for His-tagged proteins. We describe here the separation and purification of His-tagged green fluorescent protein (His-GFP) as model biomolecule, in a process that results in better capacities than industrially standard magnetic particles.

In order to improve binding capacities, a deep knowledge of some chemical and physical properties of the MNPs employed is very important. Thus, our paper goes beyond the investigation of biotechnological parameters, considering other aspects relevant for understanding and analyzing the achieved adsorption values and the correlations in the system. We report here on the structural and magnetic characterization of the magnetite nanoparticles, their long-term stability, and other elementary aspects, such as agglomeration behavior of the dispersions, availability of ligands, and the number of existing binding sites.

2. EXPERIMENTAL SECTION

2.1. Materials. Copper sulfate pentahydrate was purchased from neolab GmbH, Germany; the zinc and nickel sulfates were provided by Merck, Germany. EDTA dianhydride and methanol were purchased from Sigma-Aldrich Chemie, Germany; imidazole and Tris (Tris-(hydroxymethyl)aminomethane) were purchased from AppliChem, Germany. Acetonitrile was purchased from Avantor Performance Materials, USA. The protein marker ColorPlus Prestained from New England BioLabs, Germany was used for SDS-PAGE. All other reagents were supplied by Carl Roth, Germany. All chemical agents used were of at least analytical grade.

GFP was selected as a model protein to investigate the adsorption capacity of the MNPs. Due to its fluorescent property; it is suitable for simple analytical methods. The gene for expression of His-GFP was cloned in a pET-28a(+) vector and transformed into *E. coli* BL21 (DE3) cells. The six histidine units were placed on the C-terminus of the protein. The GFP concentration in the lysate was 8 to 9 g/L, and its content with respect to the total protein mass was about 40% (w/w).

The cells were disrupted after fermentation by high-pressure homogenization (GEA Niro, Italy). The GFP-Standard was purified from the lysate and showed a purity >98% as determined by 12% SDS PAGE and analytical reversed-phase chromatography. The protein standard was purified by IMAC, ion exchange chromatography, and size exclusion chromatography.

The solutions for the magnetic separation process were prepared in standard 0.05 M Tris buffer, pH 8.5. As wash buffer a solution of 0.05 M sodium dihydrogen phosphate (NaH_2PO_4*$2H_2O$) and 0.5 M NaCl, pH 7.9 was used. The elution buffer contained 0.05 M NaH_2PO_4*$2H_2O$, 0.5 M NaCl, and 0.5 M imidazole, pH 7.9.

2.2. Analytical Methods and Instrumentation. Metal ion quantifications of the fluids were carried out after separating the supernatants from the MNPs, and concentrations were then determined using complexometric methods (iron: 510 nm, copper: 620 nm, Infinite 200 Microplate Reader, Tecan Deutschland, Germany). The copper concentration was also measured employing *Inductively Coupled Plasma Optical Emission Spectrometry* (ICP-OES, Spectroflame, Spectro Analytical Instrument, Germany) to confirm complexometry values. Bound concentrations were then calculated by mass balance. Total determination of the mass of solids was performed using the gravimetric method; for low MNP concentrations (lower than 50 μg/mL) absorption measurements at 970 nm were used. EDTA and ligand concentrations in the MNPs were determined by nitrogen elemental analysis (*Euro EA Elemental Analyzer*, Euro Vector, Italy).

Qualitative analyses of proteins included SDS-PAGE by Coomassie staining (protein marker ColorPlus Prestained, New England BioLabs). Protein quantification was carried out by the Bradford assay with Coomassie Brillant Blue 250 according to the manufacturer's instructions using BSA as standard protein (Roti-Quant, Carl Roth GmbH & Co. KG, Germany). The GFP concentration was routinely determined using fluorescence intensity measurement (*Infinite M200 Microplate Reader*, Tecan Deutschland, Germany). The excitation wavelength was 485 nm, and the emission wavelength was 515 nm. High performance liquid chromatography, HPLC (Agilent 1100, Agilent Technologies Deutschland, Germany), equipped with a diode array detector at 220 nm was used for further protein quantification purposes and purity analysis.

Determination of hydrodynamic diameter of agglomerates and size distribution of diluted samples were performed by dynamic light scattering, DLS (Delsa Nano C, Beckman Coulter, Germany). All samples were intensively dispersed before starting the DLS-measurement. In all cases, the CONTIN algorithm values were chosen for the report, with the assumption of the Stokes−Einstein relationship for spherical particles. Zeta potential of the MNPs was measured by electrophoretic light scattering using a Delsa Nano C (Beckman

Coulter, Germany) at 298 K. Determination of morphology and size of the MNPs was carried out by transmission electron microscopy, TEM (JEM-100CX, Jeol Germany, Germany); for this purpose, diluted drops of the suspension were slowly dripped onto copper grids. Saturation magnetization measurements were conducted with a superconducting quantum interference device, SQUID (*MP MS XL-5*, Quantum Design Inc., USA) in the range 0−5 T at 300 K. Specific surface areas were calculated from BET-isotherms of nitrogen adsorption (*Gemini VII*, Micromeritics, Germany); the samples were lyophilized before measuring and further dried in the device chamber under vacuum conditions (0.05 mbar).

2.3. Nanoparticle Synthesis and Separation Sequence. The MNPs were provided by the Merck KGaA. The synthesis steps yield the following:[29]

(1) The magnetite synthesis is carried out by the continuous precipitation of iron salts ($Fe(NO_3)_3$ and $FeSO_4$) in the presence of NaOH. The two solutions from separate vessels are pumped through a mixing device, precipitating immediately in a few microliters volume at constant temperature, pH, and in the absence of oxygen.[30,31]

(2) Then a thin layer of amorphous silica is deposited by hydrolysis of tetraethoxy-silane in an alkaline suspension of magnetite particles.[32]

(3) After dispersion of the silica coated particles in an alcohol/water mixture, they are treated with a 10-fold excess of (3-glycidyloxypropyl)trimethoxysilane for several hours at 40 °C.

(4) The diamino linker is coupled with the epoxy particles on 2,4-dioxane with a 10-fold excess of the molecule referred to the expected amount of epoxy functions at elevated temperatures.[3433]

(5) The amino functionalized particles are redispersed in DMSO and react with a 5-fold excess of EDTA dianhydride over 18 h under ambient conditions. Then, wash with 200 mM phosphate buffer pH 7 and 20% ethanol takes place until a conductivity <100 μS/cm is achieved.[35]

Figure 1 schematically illustrates the structure of the EDTA-MNPs.

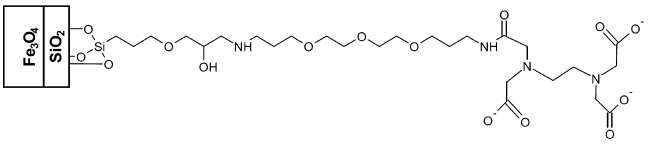

Figure 1. Schema of the magnetic nanoadsorbers with the pentadentate chelating ligand EDTA.

The synthesized core−shell MNPs showed superparamagnetic behavior. Due to this property, it is possible to separate the MNPs after each step as well as to recover them again easily when applying an external magnetic field. The main sequence for the protein isolation process from the lysate suspension includes (1) adsorption, (2) wash, (3) elution, and (4) recovery of the MNPs. During the wash steps, the target molecules remain bound to the magnetic carriers.

Next, the magnetic particles were loaded with metal ions. Metal ion solutions (0.05 M nickel(II) sulfate hexahydrate, 0.05 M copper(II) sulfate heptahydrate, or 0.05 M zinc sulfate heptahydrate, 0.5 M NaCl) were prepared and mixed with magnetic particles for 25 min. After incubation the supernatant was removed, and the particles were washed twice with 0.05 M Tris, pH 8.5.

Afterward, MNPs and lysate were incubated for 25 min in order to achieve a full saturation of the surface with target protein. After the removal of the supernatant by short centrifugation and magnetic separation, the wash buffer was added in two steps, and the suspension was mixed for 10 min. These two wash steps removed impurities and weakly bound host cell proteins. Finally the target protein was eluted in two steps. The washed magnetic nanoparticles were suspended in the elution buffer and mixed for 10 min. Elution was carried out at high concentration of imidazole (0.5 M). All experiments were performed at room temperature. For the protein adsorption isotherms, bound His-GFP concentration was calculated through addition of the total His-GFP amount from all eluted fractions.

3. RESULTS AND DISCUSSION

3.1. Nanoparticle Characterization. First, the concentration of ligand and EDTA were determined by measuring the nitrogen content in the EDTA-MNPs, assuming that all nitrogen atoms belong either to the spacer (two N atoms) or to the ligand (two more N atoms). Hence for four nitrogen atoms we expect one EDTA-ligand, as can be seen in the molecular structure in Figure 1. The MNPs contained 0.74% (w/w) nitrogen, which corresponds to 132 μmol EDTA/g MNP.

Saturation magnetization measurements of the EDTA-MNPs showed almost no hysteresis (remanence < 0.08%) and very good saturation magnetization values (≈ 59 A m^2/kg). These values correspond well with similar particles in the literature[36,37] (bulk magnetite reaches values of 90−100 A m^2/kg[38]).

Furthermore, some structural parameters of the particles were characterized using transmission electron microscopy. TEM images of the primary particles revealed their octahedral shape (Figure 2).

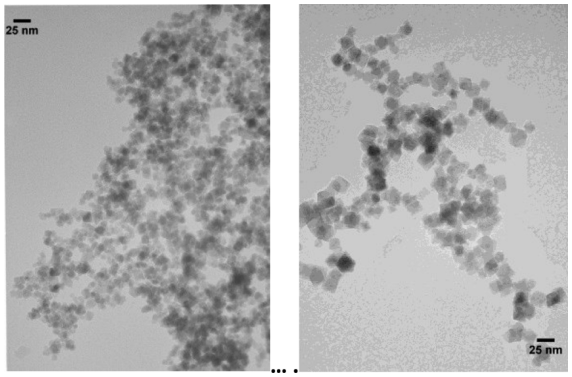

Figure 2. TEM images of EDTA-MNPs.

We considered a total of 458 particles from different TEM images for the size distribution analysis (Figure 3). These values present a monomodal distribution of particle sizes with a mean diameter x_{50} = 22 ± 4 nm; x_{10} = 17 nm, and x_{90} = 28 nm. The large number of pictures analyzed was important because of the direct relation between superparamagnetism and particle size. This narrow distribution of primary particle sizes is beneficial for technical processing since it is usually related to a lower tendency for aggregation.

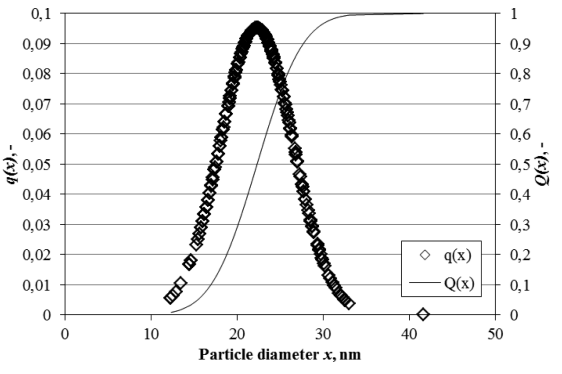

Figure 3. Differential ($q_1(x)$) and cumulative ($Q_1(x)$) size distribution functions of the primary particles.

The specific surface area of the magnetic material was determined by BET measurements on nitrogen adsorption; for the particles after the silica coating it yielded 89 m^2/g (data from Merck KGaA with permission). Further BET measurements after the reaction with spacer and ligand presented a decreased mean value of 66 m^2/g. This effect might be related to the mass change of the particles due to the attachment of organic species on their surface. We suppose that N_2 mainly adsorbs on the surface of the primary crystals but comparably little on the spacer and ligand chains. Further studies are necessary to gain a more profound understanding of the physical implications of these results.

A number of different transition metal ions are suitable for binding with the chelate ligand for the purpose of protein adsorption. We concentrated our experiments on Cu^{2+}, as we explain later (see 3.2). The loading reaction takes place immediately without any leakage of ions detected within a six month period, as we could show for the Cu^{2+}-EDTA-MNPs. The MNPs reached a maximal copper capacity of 84 μmol/g, which corresponds to a surface covering of 1.8 nm^2 per copper ion. We employed for the calculation just the nanocrystal specific surface area (89 m^2/g). Further BET measurements of the particles after the complexation with copper did not show any appreciable difference to the values without metal ion (66 m^2/g). In order to calculate the surface area available for each copper ion and, after biomolecular adsorption, for each biomolecule, it is not the surface of spacer and ligand that is relevant but only their length. These values are necessary, for example, to estimate steric hindrance effects, as shown in 3.4.

Measurements of saturation magnetization conducted after the coordination with copper ions showed very good values without relevant divergence from the ones before: 58 A m^2/kg, remanence < 0.26%.

3.2. His-GFP Adsorption. In a preliminary study we analyzed the binding capacities for His-GFP of the three divalent metal ions copper, zinc, and nickel to compare their adsorption and elution behavior. We applied here His-GFP solutions with a concentration lower than the saturation values for Ni^{2+} and Cu^{2+}. The process included just one separation step, three wash steps, and two elution steps. The experiments yielded the highest binding capacity for Cu^{2+}-loaded MNPs (Figure 4), whereas Zn^{2+}-MNPs achieved only about 17% of the Cu^{2+} capacity. Both nickel and copper showed very good selectivity and purification capacity (see Table 1).

It should be noted that after elution, 97% of the total His-GFP was recovered in the first elution step for Cu^{2+}-loaded

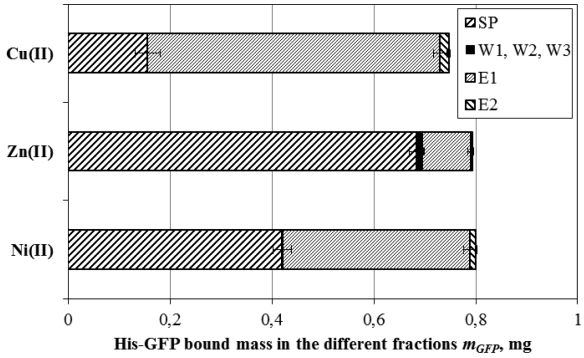

Figure 4. Comparison of His-GFP bound masses in the different fractions for the three chosen metal ions (SP, supernatant; W, wash fractions; E, elution fractions).

Table 1. Comparison of Purity Values Referred to His-GFP after One Elution Step

metal ion	purity, %
Cu^{2+}	98.7
Zn^{2+}	75.5
Ni^{2+}	94.9

MNPs. The purity results after the first elution step in Table 1 correspond to the selectivity of the ligand. Both selectivity and capacity develop consistently $Cu^{2+} > Ni^{2+} > Zn^{2+}$. Additionally, all proteins of the different processing steps were qualitatively visualized by SDS-PAGE.

In summary, the tendencies recognizable from our results are in accordance with the data of other groups in the classical chromatographic field, which also previously determined capacities for Ni^{2+}, Cu^{2+}, and Zn^{2+} usually immobilized on IDA or NTA.[39−42] The decreasing binding strength leads to decreasing adsorption values ($Cu^{2+} > Ni^{2+} > Zn^{2+}$). After these initial results, no further work was carried out with zinc particles.

For further characterization, we compared the His-GFP adsorption behavior of a purified His-GFP solution and a His-GFP containing crude cell lysate using Ni^{2+}-EDTA-MNPs and Cu^{2+}-EDTA-MNPs. The experiments were performed at pH 8.5 to ensure that the electron donor groups on the protein surface were unprotonated. Isotherms (Figure 5) and isotherm

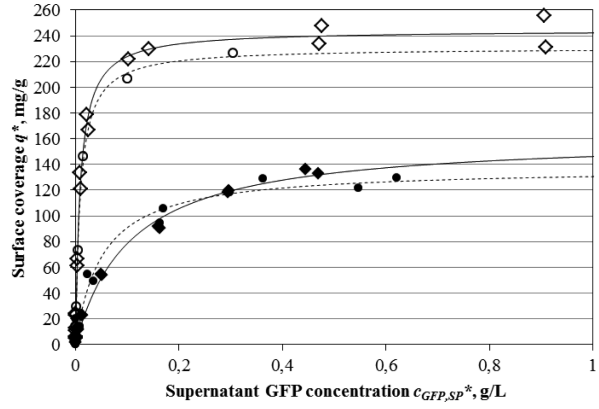

Figure 5. Adsorption isotherms of GFP on metal ion-EDTA-MNPs. *Circles*, pure compound isotherm; *rhombs*, isotherm by presence of foreign proteins; *empty symbols*, Cu-EDTA-MNPs; *filled symbols*, Ni-EDTA-MNPs. The lines represent the Langmuir adsorption model.

constants from experimental data (Table 2) fit well with the Langmuir adsorption model and enable an interpretation of monolayer surface coverage with protein when there are noninteracting binding sites on the surface.

The quality of functionalized MNPs as a separation tool depends strongly on two factors, the binding capacity and the

Table 2. His-GFP Adsorption Isotherm Constants for the Langmuir Model

adsorption isotherm	coordinated metal ion	K_d, mg/L	q_{max}, mg/g
pure compound isotherm	Cu^{2+}	9.3 (±0.8)	230.8 (±4.4)
	Ni^{2+}	51.2 (±10.4)	137.3 (±5.1)
isotherm by presence of host cell proteins	Cu^{2+}	9.2 (±0.8)	244.5 (±4.3)
	Ni^{2+}	106.2 (±7.4)	161.7 (±4.5)

selectivity for the target molecule. Our values show a significantly higher binding capacity q_{max} of the copper particles (231 mg/g) in comparison with the nickel ones (137 mg/g). The dissociation constant values K_d also yield considerably better results for Cu^{2+}-EDTA-MNPs with 5 to 6 times higher selectivity toward the target molecules when compared with the nickel ones. The slightly higher values for the lysate are deemed as within the common deviation range for such an experimental methodology and are therefore comparable to the pure compound values. For these reasons, together with the fact that copper demonstrates lower toxicity than nickel, at least for clinical applications,[43] we decided to carry out further experiments only with the copper loaded particles.

The adsorption capacity we measured is at least 10 times greater than typical values of commercial magnetic particles. Benelmekki and co-workers[44] provided a very good comparison by measuring the capacity for precisely $(His)_6$-GFP; the measurements yielded 25 mg/g with commercially available polystyrene microparticles. For comparably large proteins, the supplier reported 40 mg/g as an achievable value. Particles from other suppliers yield even lower values, e.g. 10 mg/g.[45] Our system's high capacity is due to the properties of the pentadentate ligand together with the robustness of the process.

As a final point, we want to report on the recyclability of the MNPs. The development of the His-GFP concentration after one elution step for Cu^{2+}-EDTA-MNPs was followed by a series of up to eight isolation cycles. It is a general rule in chromatographic applications to strip columns of metal ions between runs and to reload then the column again. This is usually done to remove possible contaminants entirely from the column, then loading it again with fresh ions. Because the pentadentate ligand EDTA forms very strong coordination bonds with the copper ions, we wanted to monitor in this case the loss of binding capacity with each cycle. Without reloading the particles with "new" copper ions, there is a linear decrease in bound His-GFP reaching a value of 60% of the original capacity after eight separation cycles, which is a decrease of about 5% in the capacity for each separation step. In the ninth experiment we then regenerated the particles again with copper ions and achieved 90% of the binding capacity for His-GFP. The purity of the elution fractions remained constant in all experiments and >95%. Saturation magnetization measurements conducted after many separation cycles demonstrate that the number of steps and the long-term storage of more than six months did not affect the magnetization (magnetization $\approx$ 57 A m^2/kg; remanence < 0.10%).

3.3. Assembling Behavior in the System. Regarding the performance of the separation process, control of aggregation sizes is an essential issue, since the free surface for successful binding with target molecules may depend upon it. In colloidal systems, the higher surface free energy and lower energy barriers due to the small sizes promote strong aggregation. The stability of such suspensions is governed by secondary interactions, i.e. weak intermolecular forces, such as e.g. van der Waals (VdW) interactions, hydrogen bonds, hydrophobic interactions, and screened electrostatic interactions and also magnetic dipole−dipole interactions[46] in the particular case of magnetic materials.

One special focus of this work is to analyze some basic questions related to the behavior and stability of the applied system. In this section we discuss two issues: (1) we follow the change in the system before and after loading with the metal ion and (2) we investigate the effects of different agglomeration sizes on the binding capacity. The aim is to clarify if initially formed aggregates remain stable during processing, or if stirring, for example, enables an increase in the surface area available to capture biomolecules. Is it possible to use the dynamic nature of weak intermolecular interactions as a tool for stability and faster magnetic separation, while still enhancing the available surface in the capture step with a short, energetic and homogeneous stirring treatment? This question is related to the strength of the interaction forces between adjacent MNPs in the first assemblies and in the later developing ones. Stability might also be relevant for selecting optimal storage conditions.

To avoid confusion with our terminology and following the argumentation of Nichols and co-workers,[47] we distinguish hereafter between "aggregates" (stronger bonding between particles) and "agglomerates" (loosely bound material). Nevertheless, a differentiation between them is a matter of degree, and a precise terminology remains arbitrary.

We monitored hydrodynamic size and size distribution of the agglomerates in solution after the reaction with the ligand EDTA, after the Cu^{2+}-chelate reaction, and also after the binding with His-GFP. The measurements were carried out with DLS and in some cases also with TEM. It is worth pointing out that DLS requires diluted solutions. EDTA-MNPs (before reaction with copper ions) showed, after reaching the stationary system, significantly larger aggregates than Cu^{2+}-EDTA-MNPs with polydispersity index PI $\geq$ 0.24; GFP-Cu^{2+}-EDTA-MNPs showed the same distribution of particle sizes as before GFP binding and also similar PI (see Table 3). The

Table 3. Development of Mean Hydrodynamic Diameters over Time and Adsorbed Protein Mass (in mg protein/g MNP)

sample	*D*, nm	His-GFP, mg/g
EDTA-MNP (>6 months)	430 ± 20	
Cu-EDTA-MNP (<6 months)	polydisperse system	248 ± 19
Cu-EDTA-MNP (>6 months)	225 ± 10	252 ± 13
Cu-EDTA-MNP (loading, unloading and reloading)	polydisperse system	267 ± 16
GFP-Cu-EDTA-MNP (<1 month)	235 ± 10	

charge at the surface of the particles after the reaction ligand−metal ion induces through repulsion against other particles the reduction of the mean hydrodynamic diameter. The subsequent adsorption of His-GFP does not have any further effect on the hydrodynamic values. The difference between before and after metal ion reaction is also evidenced by TEM pictures that clearly show fewer large aggregates (Figure 6) and slightly lower polydispersity. Nevertheless, PI values still remain high after loading of copper ions for most of the monitored samples due to the existence of some large assemblages also in the Cu^{2+}-MNPs, which predominantly exert influence on the results, due to the fact that the scattering intensity is proportional to the sixth power of the particle diameter.

The pictures in Figure 6 illustrate the general situation for both systems. Here, it is also important to briefly discuss the DLS-data. Number or volume distributions given through the CONTIN algorithm generally show a maximum for the Cu-EDTA-MNPs around 100 ± 10 nm or 140 ± 10 nm, respectively. These values demonstrate how strong few big

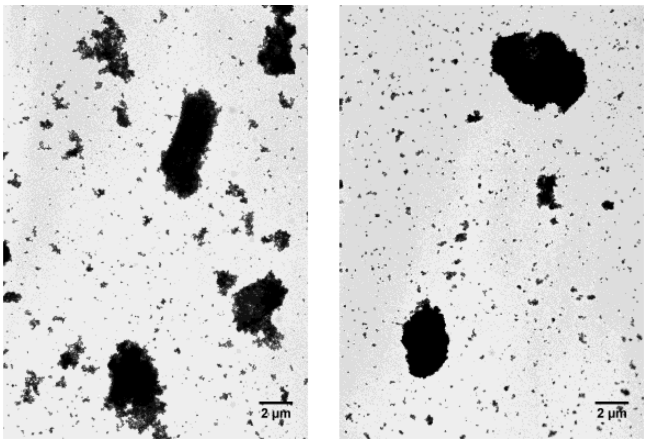

Figure 6. TEM images representative for the systems EDTA-MNPs (left side) and Cu^{2+}-EDTA-MNPs (right side).

aggregates shift the averaged intensity values to higher ones. Number and volume distributions are less sensitive than intensity ones to aggregation. This is for some analysis more in accordance with the real size distribution. DLS models calculate average data with the supposition of spherical aggregates, which is a rough approximation here, as recognizable from TEM pictures (Figure 6). It is to notice that also TEM pictures, although providing valuable information, probably give a distorted geometry of the assemblies due to the fact that the material has to be dried.

Table 3 also demonstrates that after changes on the particles' surface (loading of metal ions) long time ranges are necessary to reach constant hydrodynamic size distribution values. This means that the first, hard aggregates from the magnetite core synthesis organize fast in larger agglomerates to decrease their surface free energy and reach in a short time a sort of metastability. Probably this effect is due to the presence of local gradients after any reaction on the surface of the particles. Then, reorganization through collision and mass exchange between these agglomerates enables the system to reach slowly the final stable hydrodynamic size distribution. This stabilization involves higher homogeneity and a decrease in mean sizes, although some big aggregates still remain in solution.

As regards the stability of nanodispersions, the zeta potential can also yield valuable information.[48] We carried out measurements in the Tris buffer solution (pH 8.4), and the tendency was for both EDTA-MNPs and Cu-EDTA-MNPs to be around −25 mV. The values in water were generally lower and strongly dependent on the remaining electrolyte concentration. These results confirm that the particles are more stable in the buffer solution than in water.

From a biotechnological point of view, an analysis of the aggregation and agglomeration behavior is only important in relation to its effects on the binding capacity. Therefore, we measured the maximum capacities for His-GFP of the MNPs in the different time intervals. As can be seen in Table 3 all experiments with the Cu-EDTA-MNPs reached comparable values for adsorbed His-GFP.

The constant values of the bound His-GFP concentration in Table 3 for large differences in the existing hydrodynamic size distribution demonstrate that the forces acting between the agglomerates are weak enough to be broken up by a short stirring step, so that the available surface can successfully be reached by the target molecules, in our case the histidine residues attached to GFP. This means that in later steps of the nanoparticles' synthesis (ligand attachment and loading with metal ions), softer interactions govern the distribution of sizes in the system, but these interactions do not influence adsorption capacity. On the other hand, aggregation of the primary particles, together with the results of the posterior synthesis steps (silica layer and eventually also the spacer chains), affects the final capacity (see section 3.4).

3.4. Binding Sites. One of the critical weaknesses of magnetic particles as a bioseparation tool is the complex and expensive production process which yields comparatively lower binding capacities than expected. For a given material mass, the total surface area increases enormously when particle size decreases to the nanometer scale. Even though the specific surface area is then very high, aggregation often leads to a very low fraction of this area remaining free enough to be reached by the target molecules during the binding step. This is also observable in our system: there exists a remarkable discrepancy between the theoretical capacity of our MNPs and the measured adsorption values at the end of the separation process. Thus, we analyze here the reasons for this divergence. We define theoretical capacity as the expected value in a calculation with regard to the available area of the primary MNPs and the coverage with binding sites.

The following calculations were carried out only for the system with copper ions. For $(His)_6$-GFP we presume a mass of 28 kDa.[49] The analysis of concentrations yields an estimation of the maximal protein binding capacity expected from the process with the assumption that each ligand builds a complex with just one Cu^{2+}-ion and that at most one His-GFP binds to each Cu^{2+}-ion. In section 3.1 we already presented the values for the EDTA and Cu^{2+} concentrations. Table 4 shows the relation between the concentrations of chelating agent, metal ion, and bound protein.

Table 4. Loss of Binding Capacity[a]

	$c_{exp,i}$, µmol/g	$c_{exp,i}/c_{EDTA}$, %
Cu^{2+}	84	64
GFP	8.7	6.6

[a]Comparison between measured ($c_{exp,i}$) and expected ($c_{exp,i}/c_{EDTA}$) values.

The values in Table 4 show that (1) 64% of the ligands formed a complex with copper ions and (2) ten metal ions were necessary to bind one His-GFP. The final His-GFP concentration therefore reaches merely between 0.1 and 0.01 of the expected result.

The loss of binding sites in each step of the synthesis and the discrepancy between expected and measured values is common in any synthesis process and can result from different reasons, mainly related to the incomplete conversion rates during the different steps. The nitrogen content generates information on both, the ligand and the spacer, without enabling a separate quantification of each and thus a separate discussion. Nevertheless the highest loss of capacity concerns the low fraction of reachable copper ions for the protein molecules due to steric hindrance. Steric hindrance does not only mean hindrance of the His-GFP molecules among themselves but more importantly the fact that many metal ions are inaccessible for the protein due to the aggregation of the primary particles. This fact is suggested by the results presented in section 3.3 together with the discussion below.

Frankamp and collaborators studied interparticle interactions for similar magnetite nanoparticles to ours, governed mainly by magnetic polarization effects,[50] and calculated edge-to-edge spacing of just 1 nm; other authors published values of <2 nm.[51,52] Our iron oxide cores are larger than the ones in the literature studies, so they might have a higher magnetic moment per particle; thus, this value might vary by several angstroms, but it will still be considerably lower than the His-GFP dimensions. These findings are the starting point for our argumentation, that the assembly of primary MNPs into stable aggregates by adhesion forces between neighboring particles does not enable a molecule as big as His-GFP to enter. The GFP has a volume of about 19 nm^3 (about 1000 times the volume of the N_2 molecule) and cross sectional areas of about 10 nm^2 (rectangular section) and 4.5 nm^2 (circular section)[53] (0.16 nm^2 for N_2).

To summarize and refer again to the discussion in section 3.3, two structurally different assembly levels are recognizable in the system:

a) A hard assembly of the primary iron oxide nanoparticles which remains stable through the different functionalization steps on their shell and during the whole separation process, forming a barrier to the protein.

b) A soft assembly of the hard aggregates into larger agglomerates during the synthesis steps of the nanoparticles' shell, which does not affect the accessibility to the copper ions for the His-GFP. The available sites would include just the external copper ions of the aggregates addressed above.

If we compare the diameter values for the Cu^{2+}-EDTA-MNPs (final diameter, approximately 30 nm) and the mean hydrodynamic diameter of the aggregates (mean DLS diameter, ca. 225 nm) we obtain a relation close to the values between the copper and the His-GFP concentrations. While it might be a rough approximation, it is conceivable that a relation between these values exists. The relation aggregate volume (V_{ag}) to MNP volume (V_{MNP}), V_{ag}/V_{MNP}, corresponds to the number of MNPs in one aggregate (N_{MNP}). Due to the homogeneous distribution of copper ions in the MNPs, N_{MNP} is directly proportional to the number of Cu^{2+} ions in the aggregate and to its concentration, $c_{Cu,total}$. The relation surface area of the aggregate (A_{ag}) to surface area of the MNP (A_{MNP}), A_{ag}/A_{MNP}, yields the number of particles, whose added surface areas account for the total area of the aggregate ($N_{MNP,A}$). This relation is directly proportional to the number or concentration of Cu^{2+} on the free attainable surface, $c_{Cu,available}$.

$$\frac{V_{ag}}{V_{MNP}} = N_{MNP} \approx c_{Cu,total} \quad (1)$$

$$\frac{A_{ag}}{A_{MNP}} = N_{MNP,A} \approx c_{Cu,available} \quad (2)$$

$$\frac{\frac{A_{ag}}{A_{MNP}}}{\frac{V_{ag}}{V_{MNP}}} \approx \frac{c_{Cu,available}}{c_{Cu,total}} \quad (3)$$

If we assume here that the magnetic aggregates as well as their agglomerates can be considered approximately spherical, then it is possible to simplify the relation 3 as

$$\frac{\frac{A_{ag}}{A_{MNP}}}{\frac{V_{ag}}{V_{MNP}}} = \frac{r_{MNP}}{r_{ag}} \approx \frac{c_{Cu,available}}{c_{Cu,total}} \quad (4)$$

The ratio r_{MNP}/r_{ag} gives an estimation value of the number of copper ions reachable for a His-GFP molecule related to the total ones (see the schematic representation in Figure 7) and so

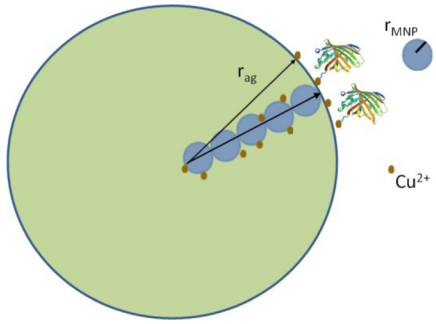

Figure 7. Schematic representation of an aggregate of MNPs and the relation between the particles accounting for an effective adsorption of His-GFP and the particles inside the aggregate, which are not accessible for the protein.

a simple approach to calculating achievable binding capacities and their relationship to the ligand concentrations (in this case, to the metal ion as the last capture step). There are however some weaknesses to this approach:

- Neither nanoparticles nor aggregates have a spherical shape. This approximation for the aggregates is quite different from reality: they might have significantly higher surface area. Furthermore, their shape is not homogeneous.
- The aggregates mean diameter is taken from the intensity distribution values (DLS measurements, CONTIN algorithm) as probably the closest one to a real description of the system. Nevertheless, it should be mentioned again that it is difficult to know if number or volume distributions could provide more significant values. Further investigation would be necessary to clarify this question. In any case, the diameter values would still remain higher than 100 nm. Possible values for the ratio r_{MNP}/r_{ag} would then be $1:5 < r_{MNP}:r_{ag} < 1:15$, so that a realistic final protein capacity would approximately reach between 5% and 20% of the immobilized metal ion concentration.

Despite the fact that these calculations are based on many assumptions, they provide insights into the difference of magnitude between possible binding sites and actual capture interactions in the real system. This is an attempt to address an issue critical for all bioseparation studies: the boundary between a "hard" aggregation which prevents the binding capacity and a "soft" agglomeration which does not influence it. We make an effort to discern between these two different interaction levels.

One last point should still be mentioned to better understand the measured protein capacities. If we calculate the surface area of a sphere of radius including core, spacer, chelate ligand, metal ion, and also the 6 His units (the histidine chain increases the binding distance and therefore also the available surface for each protein), then the occupational density of binding sites is close to 1 protein site/3 nm^2 MNP. If the GFP cross section is 4.5 nm^2, steric hindrance between GFP molecules is likely to reduce the number of proteins attaching to copper ions on the available surface. Additionally we carried out experiments in which we compared the development of the bound His-GFP

concentration with the bound copper concentration: the protein reaches its saturation capacity at about 65% of the copper saturation value, after that remaining constant with further increase of the bound copper concentration. This fact corresponds well with the steric hindrance of the protein molecules among themselves. Preliminary studies of the binding capacity of the amino acid histidine (with a cross sectional area smaller than 1 nm^2) confirm that the steric hindrance among proteins is also responsible for a reduction of the maximal capacity for His-GFP. Histidine binds around 80% more than His-GFP. This result reinforces our theory that the steric effect is of secondary importance when compared to the effect of aggregation in reducing capacity values. This means as well that the aggregates are packed tightly enough to also stop histidine units from entering. Reproduction of the first results with histidine and further studies with other molecules are necessary to further clarify these issues.

4. CONCLUSIONS AND OUTLOOK

Enhanced design of magnetic nanoparticles is an important topic in current research on biomolecular separation. Scientists are still searching for easy and fast processing steps with higher capacities and better selectivity than possible nowadays. In this context, we present in this paper a broad analysis of one concrete system, considering the relationship between biotechnological aspects and material properties as a way to understand how different effects impact final protein recovery. We report on the application of a special immobilized metal ion affinity system formed by a core of magnetite nanoparticles functionalized with a pentadentate chelate ligand that differs from classical systems based on IDA and NTA ligands. Copper ions yielded the best results (250 mg/g) in comparison with zinc and nickel ions for the separation of $(His)_6$-GFP from an unclarified *E. coli* cell lysate. The MNPs remain absolutely stable for long time periods. Moreover, good reusability of the sorbents over several purification cycles as well as very fast binding and elution kinetics were achieved. The results show that the applied nanoparticles offer attractive advantages for potential implementation in industrial biocapture processes. In future publications we aim to show that this is a very interesting alternative to established systems for an industrial downstreaming by means of magnetic separation.

The work includes the characterization of the main physical properties of the particles. These are high saturation magnetization, high specific surface area, monodisperse primary particle distribution with small mean radius, and the stability of the aggregated system. In a time scale of some months, the final system (Cu^{2+}-EDTA-MNPs) reaches a stationary distribution of hydrodynamic sizes. We presume that the mean size values remain close to the values of the assembled nanoparticles after the core synthesis. Later functionalization steps lead to further and softer agglomeration levels that have no effect on protein capture.

To summarize, the separation capacity in the case of His-GFP is essentially dependent on the available surface area and naturally on the density of the binding sites on this area. Markedly different agglomeration states in our system lead to the same capacity, so that capacity is not governed by weak agglomeration forms. Instead, the strong aggregation of the initial iron oxide particles cannot be changed without strong energetic sources, and this is the real barrier to higher capacity values because most of the metal ions remain inaccessible for interaction with the protein. We make an attempt to correlate aggregation with adsorption capacity, both of them critical aspects for any downstream application with MNPs. Thus, it is necessary to find ways of preventing the aggregation of the primary MNPs or to develop new synthesis routes which make it possible to reach all interaction sites. Mesoporous iron oxide nanoparticles might represent an interesting alternative. In connection with metal removal from contaminated waters, a slightly higher removal capacity has already been experimentally demonstrated.[54] However, the synthesis is much more complicated and must be further optimized. Moreover, the problem of accessibility for molecules as large as proteins will probably remain unresolved, since they are not likely to diffuse fast and unhindered in the mesopores. Porous hollow MNPs with pores of ~2−4 nm have been applied for the controlled release of molecules,[55] although it seems difficult to obtain sufficient porosity to be penetrable for molecules.[56]

Two fundamental issues remain unanswered in our work: (1) the hydrodynamic size distribution after the steps in the synthesis of the MNPs and (2) the value of the interparticle separation distances. Both subjects are central topics for further study.

As far as we know, this is the first journal article reporting on the application of a "pentadentate" magnetic carrier for bioseparation. The main advantage of this approach is the easy and fast separation by magnetic forces which also leads to high capacity, selectivity, and purity of the process.

■ ASSOCIATED CONTENT

Supporting Information

Additional information details about saturation magnetization, SDS PAGE of the collected fractions after a separation process, and the adsorption capacity of the particles after recycling. This material is available free of charge via the Internet at http://pubs.acs.org.

■ AUTHOR INFORMATION

Corresponding Author

*E-mail: s.berensmeier@tum.de.

Notes

The authors declare no competing financial interest.

■ ACKNOWLEDGMENTS

We gratefully thank Dr. Johann Bauer (Merck KGaA) for providing the EDTA-MNPs. We also thank Christian Roth for some TEM pictures and for the SQUID measurements.

■ REFERENCES

(1) Porath, J.; Carlsson, J.; Olsson, I.; Belfrage, G. Metal Chelate Affinity Chromatography, A New Approach to Protein Fractionation. *Nature* **1975**, *258*, 598−599.

(2) Chaga, G. S. Twenty-Five Years of Immobilized Metal Ion Affinity Chromatography: Past, Present and Future. *J. Biochem. Biophys. Methods* **2001**, *49*, 313−334.

(3) Gaberc-Porekar, V.; Menart, V. Potential for Using Histidine Tags in Purification of Proteins at Large Scale. *Chem. Eng. Technol.* **2005**, *28*, 1306−1314.

(4) Loennerdal, B.; Keen, C. L. Metal Chelate Affinity Chromatography of Proteins. *J. Appl. Biochem.* **1982**, *4*, 203−208.

(5) Porath, J. Immobilized Metal Ion Affinity Chromatography. *Protein Expression Purif.* **1992**, *3*, 263−281.

(6) Zhu, J.; Sun, G. Facile Fabrication of Hydrophilic Nanofibrous Membranes with an Immobilized Metal−Chelate Affinity Complex for Selective Protein Separation. *ACS Appl. Mater. Interfaces* **2014**, *6*, 925−932.

(7) Hochuli, E.; Bannwarth, W.; Doebeli, H.; Gentz, R.; Stueber, D. Genetic Approach to Facilitate Purification of Recombinant Proteins with a Novel Metal Chelate Adsorbent. *Bio/Technology* **1988**, *6*, 1321−1325.
(8) Nakamura, I.; Makino, A.; Ohmae, M.; Kimura, S. Immobilization of His-Tagged Endoglucanase on Gold via Various Ni-NTA Self-Assembled Monolayers and Its Hydrolytic Activity. *Macromol. Biosci.* **2010**, *10*, 1265−1272.
(9) Yip, T. T.; Nakagawa, Y.; Porath, J. Evaluation of the Interaction of Peptides with Copper(II), Nickel(II), and Zinc(II) by High-Performance Immobilized Metal Ion Affinity Chromatography. *Anal. Biochem.* **1989**, *183*, 159−171.
(10) Young, C. L.; Britton, Z. T.; Robinson, A. S. Recombinant Protein Expression and Purification: A Comprehensive Review of Affinity Tags and Microbial Applications. *Biotechnol. J.* **2012**, *7*, 620−634.
(11) McCurley, M. F.; Seitz, W. R. The Nature of Immobilized Tris(carboxymethyl)ethylenediamine. *Talanta* **1989**, *36*, 341−346.
(12) Haner, M.; Henzl, M. T.; Raissouni, B.; Birnbaum, E. R. Synthesis of a New Chelating Gel: Removal of Calcium Ions from Parvalbumin. *Anal. Biochem.* **1984**, *138*, 229−234.
(13) Patchornik, G. Purification of His-Tagged Proteins with [Desthiobiotin−BSA−EDTA] Conjugates Exhibiting Resistance to EDTA. *Bioconjugate Chem.* **2008**, *19*, 673−679.
(14) Andersson, L. C.; Arefalk, A.; Lind, O.; Noren, B. *Method for Preparation of a Biomolecule Adsorbent for the Purification of Proteins by IMAC* (WO2009008802A1).
(15) Andersson, L. C.; Belew, M.; Gebru, T.; Glad, G.; Lindgren, H.; Norrman, N. *A Method of Preparing an Immobilized Metal Ion Chromatography Adsorbent and Methods of Purifying Proteins, Peptides or Polynucleotides* (WO2007139470A1).
(16) Algotsson, M.; Andersson, L. C.; Brekkan, E.; Hedemyr, L.; Maloisel, J.-L.; Palmgren, R. *Novel Chelator and Use Thereof* (WO2011152782A1).
(17) Franzreb, M.; Siemann-Herzberg, M.; Hobley, T. J.; Thomas, O. R. T. Protein Purification using Magnetic Adsorbent Particles. *Appl. Microbiol. Biotechnol.* **2006**, *70*, 505−516.
(18) Gupta, A. K.; Gupta, M. Synthesis and Surface Engineering of Iron Oxide Nanoparticles for Biomedical Applications. *Biomaterials* **2005**, *26*, 3995−4021.
(19) Laurent, S.; Forge, D.; Port, M.; Roch, A.; Robic, C.; Vander Elst, L.; Muller, R. N. Magnetic Iron Oxide Nanoparticles: Synthesis, Stabilization, Vectorization, Physicochemical Characterizations, and Biological Applications. *Chem. Rev.* **2008**, *108*, 2064−2110.
(20) Iida, H.; Takayanagi, K.; Nakanishi, T.; Osaka, T. Synthesis of Fe_3O_4 Nanoparticles with Various Sizes and Magnetic Properties by Controlled Hydrolysis. *J. Colloid Interface Sci.* **2007**, *314*, 274−280.
(21) Jolivet, J.-P; Chanéac, C.; Tronc, E. Iron Oxide Chemistry. From Molecular Clusters to Extended Solid Networks. *Chem. Commun.* **2004**, 481−487.
(22) Guo, J.; Yang, W.; Wang, C. Magnetic Colloidal Supraparticles: Design, Fabrication and Biomedical Applications. *Adv. Mater.* **2013**, 1−19.
(23) Liu, Z.; Li, M.; Pu, F.; Ren, J.; Yang, X.; Qu, X. Hierarchical Magnetic Core-Shell Nanoarchitectures: Non-Linker Reagent Synthetic Route and Applications in a Biomolecule Separation System. *J. Mater. Chem.* **2012**, *22*, 2935−2942.
(24) Liu, X.; Guan, Y.; Liu, H.; Ma, Z.; Yang, Y.; Wu, X. Preparation and Characterization of Magnetic Polymer Nanospheres with High Protein Binding Capacity. *J. Magn. Magn. Mater.* **2005**, *293*, 111−118.
(25) Ma, Z. Y.; Guan, Y. P.; Liu, X. Q.; Liu, H. Z. Synthesis of Magnetic Chelator for High-Capacity Immobilized Metal Affinity Adsorption of Protein by Cerium Initiated Graft Polymerization. *Langmuir* **2005**, *21*, 6987−6994.
(26) Odabasi, M.; Uzun, L.; Denizli, A. Porous Magnetic Chelator Support for Albumin Adsorption by Immobilized Metal Affinity Separation. *J. Appl. Polym. Sci.* **2004**, *93*, 2501−2510.
(27) Li, Y.-C.; Lin, Y.-S.; Tsai, P.-J.; Chen, C.-T.; Chen, W.-Y.; Chen, Y.-C. Nitrilotriacetic Acid-Coated Magnetic Nanoparticles as Affinity Probes for Enrichment of Histidine-Tagged Proteins and Phosphorylated Peptides. *Anal. Chem.* **2007**, *79*, 7519−7525.
(28) ShiXing, W.; Sun, W.; Zhou, Y. Preparation of Cu^{2+}/NTA-Derivatized Branch Polyglycerol Magnetic Nanoparticles for Protein Adsorption. *J. Nanopart. Res.* **2010**, *12*, 2467−2472.
(29) Bauer, J.; Holschuh, K. Industrial Production, Surface Modification, and Application of Magnetic Particles. In *Upscaling of Bio-Nano-Processes*; Nirschl, H., Keller, K., Eds.; Springer: Berlin, Heidelberg, 2014.
(30) Massart, R. Preparation of Aqueous Magnetic Liquids in Alkaline and Acidic Media. *IEEE Trans. Magn.* **1981**, *17*, 1247−1248.
(31) Sugimoto, T.; Matijevic, E. Formation of Uniform Spherical Magnetite Particles by Crystallization from Ferrous Hydroxide Gels. *J. Colloid Interface Sci.* **1980**, *74*, 227−243.
(32) Stöber, W.; Fink, A.; Bohn, E. Controlled Growth of Monodisperse Silica Spheres in the Micron Size Range. *J. Colloid Interface Sci.* **1968**, *26*, 62−69.
(33) Saal, K. *Surface Silanization and Its Application in Biomolecule Coupling*. Ph.D. Thesis, Tartu University, 2006.
(34) Rozenberg, B. A. Kinetics, Thermodynamics and Mechanism of Reactions of Epoxy Oligomers with Amines. In *Epoxy Resins and Composites II*; Dusek, K., Eds.; Springer: Berlin, Heidelberg, 1986; Vol. 75, pp 113−165.
(35) Takeshita, T.; Shimoara, T.-A.; Maeda, S. Synthesis of EDTA-Monoalkylamide Chelates and Evaluation of the Surface-Active Properties. *J. Am. Oil Chem. Soc.* **1982**, *59*, 104−107.
(36) Zheng, J.; Ma, C.; Sun, Y.; Pan, M.; Li, L.; Hu, X.; Yang, W. Maltodextrin-Modified Magnetic Microspheres for Selective Enrichment of Maltose Binding Proteins. *ACS Appl. Mater. Interfaces* **2014**, *6*, 3568−3574.
(37) Santoyo Salazar, J.; Perez, L.; De Abril, O.; Truong Phuoc, L.; Ihiawakrim, D.; Vazquez, M.; Greneche, J.-M.; Begin-Colin, S.; Pourroy, G. Magnetic Iron Oxide Nanoparticles in 10−40 nm Range: Composition in Terms of Magnetite/Maghemite Ratio and Effect on the Magnetic Properties. *Chem. Mater.* **2011**, *23*, 1379−1386.
(38) Lu, A.-H.; Salabas, E. L.; Schüth, F. Magnetic Nanoparticles: Synthesis, Protection, Functionalization, and Application. *Angew. Chem., Int. Ed.* **2007**, *46*, 1222−1244.
(39) O'Brien, S. M.; Sloane, R. P.; Thomas, O. R.; Dunnill, P. Characterisation of Non-Porous Magnetic Chelator Supports and their Use to Recover Polyhistidine-Tailed T4 Lysozyme from a Crude E. Coli Extract. *J. Biotechnol.* **1997**, *54*, 53−67.
(40) Jiang, W.; Prescott, M.; Devenish, R. J.; Spiccia, L.; Hearn, M. T. W. Separation of Hexahistidine Fusion Proteins with Immobilized Metal Ion Affinity Chromatographic (IMAC) Sorbents Derived from M(N+)-tacn and Its Derivatives. *Biotechnol. Bioeng.* **2009**, *103*, 747−756.
(41) Graham, B.; Spiccia, L.; Hearn, M. T. W. Comparison of the Binding Behavior of Several Histidine-Containing Proteins with Immobilized Copper(II) Complexes of 1,4,7-triazacyclononane and 1,4-bis(1,4,7-triazacyclononan-1-yl)butane. *J. Chromatogr., B: Anal. Technol. Biomed. Life Sci.* **2011**, *879*, 844−852.
(42) Chiang, C.-L.; Chen, C.-Y.; Chang, L.-W. Purification of Recombinant Enhanced Green Fluorescent Protein Expressed in Escherichia Coli with New Immobilized Metal Ion Affinity Magnetic Absorbents. *J. Chromatogr., B: Anal. Technol. Biomed. Life Sci.* **2008**, *864*, 116−122.
(43) Casey, J. L.; Keep, P. A.; Chester, K. A.; Robson, L.; Hawkins, R. E.; Begent, R. H. J. Purification of Bacterially Expressed Single Chain Fv Antibodies for Clinical Applications Using Metal Chelate Chromatography. *J. Immunol. Methods* **1995**, *179*, 105−116.
(44) Benelmekki, M.; Xuriguera, E.; Caparros, C.; Rodríguez-Carmona, E.; Mendoza, R.; Corchero, J.; Lanceros-Mendez, S.; Martinez, L. Design and Characterization of Ni^{2+} and Co^{2+} Decorated Porous Magnetic Silica Spheres Synthesized by Hydrothermal-Assisted Modified-Stöber Method for His-Tagged Proteins Separation. *J. Colloid Interface Sci.* **2012**, *365*, 156−162.
(45) Xu, C.; Xu, K.; Gu, H.; Zhong, X.; Guo, Z.; Zheng, R.; Zhang, X.; Xu, B. Nitrilotriacetic Acid-Modified Magnetic Nanoparticles as a

General Agent to Bind Histidine-Tagged Proteins. *J. Am. Chem. Soc.* **2004**, *126*, 3392−3393.
(46) Koksharov, Y. A. Magnetism of Nanoparticles: Effects of Size, Shape and Interactions. In *Magnetic Nanoparticles*; Gubin, S. P., Eds.; Wiley-VCH: Weinheim, 2009; pp 223−227.
(47) Nichols, G.; Byard, S.; Bloxham, M. J.; Botterill, J.; Dawson, N. J.; Dennis, A.; Diart, V.; North, N. C.; Sherwood, J. D. A Review of the Terms Agglomerate and Aggregate with a Recommendation for Nomenclature Used in Powder and Particle Characterization. *J. Pharm. Sci.* **2002**, *91*, 2103−2109.
(48) Masthoff, I.-C.; David, F.; Wittmann, C.; Garnweitner, G. Functionalization of Magnetic Nanoparticles with High-Binding Capacity for Affinity Separation of Therapeutic Proteins. *J. Nanopart. Res.* **2014**, *16*, 2164.
(49) Ward, W. W. Biochemical and Physical Properties of Green Fluorescent Protein. In *Green Fluorescent Protein*; Chalfie, M., Kain, S. R., Eds.; John Wiley & Sons, Inc.: Hoboken, NJ, USA, 2005; pp 39−65.
(50) Frankamp, B. L.; Boal, A. K.; Tuominen, M. T.; Rotello, V. M. Direct Control of the Magnetic Interaction between Iron Oxide Nanoparticles through Dendrimer-Mediated Self-Assembly. *J. Am. Chem. Soc.* **2005**, *127*, 9731−9735.
(51) Voggu, R.; Kumar, N.; Rao, C. N. R. Dependence of the Properties of Magnetic Nanoparticles on the Interparticle Separation. *J. Phys. Chem. C* **2008**, *112*, 17775−17777.
(52) Yang, H. T.; Hasegawa, D.; Takahashi, M.; Ogawa, T. Achieving a Noninteracting Magnetic Nanoparticle System through Direct Control of Interparticle Spacing. *Appl. Phys. Lett.* **2009**, *94*, 13103.
(53) Ormö, M.; Cubitt, A. B.; Kallio, K.; Gross, L. A.; Tsien, R. Y.; Remington, S. J. Crystal Structure of the Aequorea Victoria Green Fluorescent Protein. *Science* **1996**, *273*, 1392−1395.
(54) Liu, M.; Wen, T.; Wu, X.; Chen, C.; Hu, J.; Li, J.; Wang, X. Synthesis of Porous Fe_3O_4 Hollow Microspheres/Graphene Oxide Composite for Cr(VI) Removal. *Dalton Trans.* **2013**, *42*, 14710.
(55) Cheng, K.; Peng, S.; Xu, C.; Sun, S. Porous Hollow Fe_3O_4 Nanoparticles for Targeted Delivery and Controlled Release of Cisplatin. *J. Am. Chem. Soc.* **2009**, *131*, 10637−10644.
(56) Podsiadlo, P.; Kwon, S. G.; Koo, B.; Lee, B.; Prakapenka, V. B.; Dera, P.; Zhuravlev, K. K.; Krylova, G.; Shevchenko, E. V. How "Hollow" Are Hollow Nanoparticles? *J. Am. Chem. Soc.* **2013**, *135*, 2435−2438.